Control of beaming angles via a subwavelength metallic slit surrounded by grooves

W. Dai
Ames Laboratory, U.S. DOE, and Department of Physics and Astronomy, Iowa State University, Ames, Iowa 50011, USA

C. M. Soukoulis*
Ames Laboratory, U.S. DOE, and Department of Physics and Astronomy, Iowa State University, Ames, Iowa 50011, USA and Institute of Electronic Structure and Lasers (IESL), FORTH, and Department of Material Science and Technology, University of Crete, 71110 Heraklion, Crete, Greece

(Received 20 November 2009; revised manuscript received 7 July 2010; published 26 July 2010)

We are studying a subwavelength slit in a lossy metal film illuminated by electromagnetic waves. Periodic grooves are placed on the output side surrounding the slit. Surface plasmons along the metallic surface on the output side are excited by the electromagnetic wave propagating through the slit. The grooves modulate the surface plasmons and couple them into propagation modes, which facilitates the beaming of the output field. We developed an efficient method to determine the geometric parameters of the grooves that are necessary to achieve oblique beaming at any angle between 0 and 70 degrees. We also designed a frequency splitter by setting appropriate parameters of the grooves.

DOI: 10.1103/PhysRevB.82.045427 PACS number(s): 78.66.Bz, 73.20.Mf, 42.25.Fx, 42.25.Bs

Normally the light coming out a subwavelength waveguide will be diffracted to all angles. With the help of surface waves along the output surface, the emitted light can be confined in a small angle range. This phenomenon is called beaming and was discovered in 2002.[1] Since then, it has been studied extensively experimentally and theoretically using metallic structures[1–6] or photonic crystals.[7–11]

Beside the research on forward beaming mentioned above, oblique beaming was also demonstrated using either metallic structures[12–14] or photonic crystals.[15] Obviously it is important to control the beaming angle of the oblique beaming freely. In this paper, we present an efficient method to design a metallic structure which will steer the emitted field to any given angle. We also find the best beaming happens at an oblique direction.

Figure 1 shows the structure studied in the paper: a metallic subwavelength slit surrounded by grooves. It is an important plasmonic structure.[16] As a two-dimensional structure, it can be solved analytically and serves as a theoretical model to understand the physics of beaming.[2] It is a multifunctional beaming structure. It can achieve intermediate-field beaming,[3] far-field beaming,[2] and specially far-field oblique beaming which will be studied here. The near-field focusing was also implemented by similar structures.[20] Grooves at the input surface can enhance the transmission dramatically,[17,18] so this structure can improve transmission and directionality of the output field simultaneously.[12] Recently this structure was integrated with a semiconductor laser to converge the emitted fields.[19]

Since electromagnetic fields decay rapidly inside the metal, the metal can be "replaced" by surface impedance boundary conditions (SIBC),[21] which states the electromagnetic fields at the metal surface satisfy

$$E_{\parallel} = Z\hat{n} \times H_{\parallel}, \quad Z = \sqrt{\mu_m \mu_0 / \epsilon_m \epsilon_0}.$$

Here $\hat{n}$ is the normal unit vector pointing out of the metal; $E_{\parallel}$ and $H_{\parallel}$ are components of electric and magnetic fields

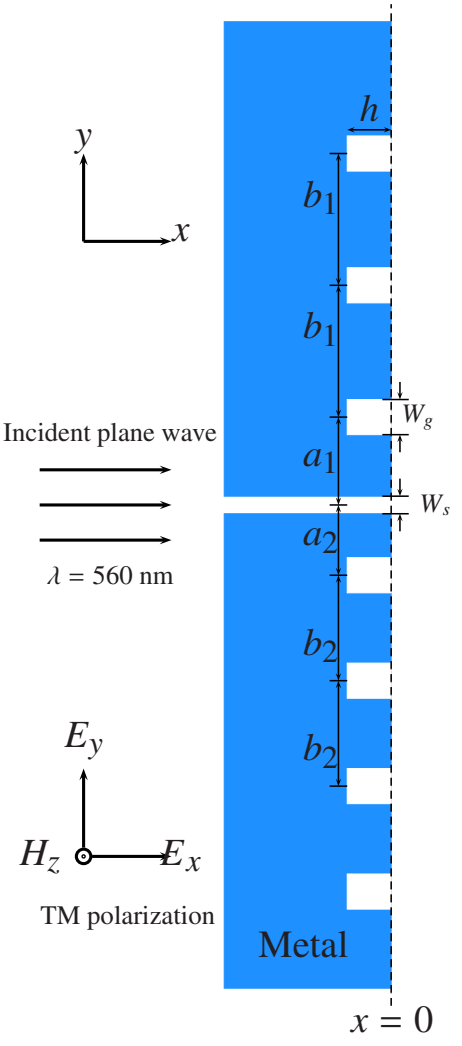

FIG. 1. (Color online) Schematic representation of the subwavelength metal slit surrounded by upper and lower periodic grooves embedded in free space.

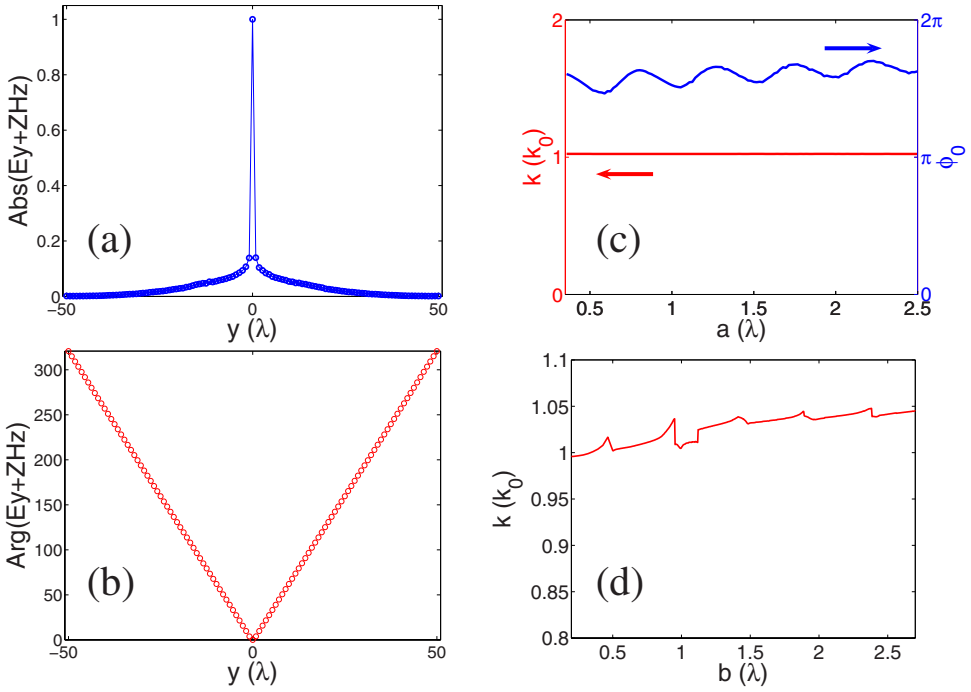

FIG. 2. (Color online) (a) and (b) Amplitudes and phases of fields at symmetric grooves with $a=b=500$ nm; (c) and (d) the linear fitting results of phases of the fields at grooves for different a when (c) $b=500$ nm and for different b when (d) $a=500$ nm.

parallel to the metal surface. Z is the impedance of the metal; ϵ_m and μ_m are relative permittivity and permeability of the metal; ϵ_0 and μ_0 are vacuum permittivity and permeability.

The coordinate system is defined in Fig. 1. $x=0$ is the output surface of the slit. When the incident wave is TE polarized (the nonzero components of the electromagnetic fields are H_z, E_x, and E_y), surface plasmons exist at the metal surface. In this paper, we focus on the fields at and after the output surface of the slit. At the output surface, the SIBC becomes

$$E_y + ZH_z = 0.$$

Define $F=E_y+ZH_z$. Given the F field along $x=0$, we can calculate the electric and magnetic fields at any points in the $x>0$ half-plane. Define the far-field angular transmission $P(\theta)$ as

$$P(\theta) = \lim_{r\to\infty} r|\vec{S}(\vec{r})|, \tag{1}$$

where $\vec{S}(\vec{r})$ is the Poynting vector at the point $\vec{r}=(r\sin\theta, r\cos\theta)$. Then the total transmission T is

$$T = \int_{-\pi/2}^{\pi/2} P(\theta)d\theta,$$

and $P(\theta)$ can be calculated from the F fields as

$$P(\theta) = \frac{k_0}{2Z_0}\left|\frac{\cos\theta}{\cos\theta + Z/Z_0}\right|^2 \left|\int_{-\infty}^{\infty} dy' F(0,y')e^{-ik_0 \sin\theta y'}\right|. \tag{2}$$

Here we assume the $x>0$ half-plane is free space; k_0 and Z_0 are the wave vector and the impedance in free space. Then we define the normalized far-field angular transmission as $I(\theta)=P(\theta)/T$ and use it to describe the far-field distribution.

Because of the surface impedance boundary condition, the F field along $x=0$ is zero except the opening area of the slit and grooves. Since the widths of the indentations (slit and grooves) are much smaller than the incident wavelength, we assume the field is constant inside an indentation and Eq. (2) is approximately the summation of several point sources. We will define the F field at the ith grooves as F_i; positive i means the groove above the slit, negative i means the groove below the slit and $i=0$ represents the slit. In this paper, F_i are obtained by using the finite element method software COMSOL Multiphysics. They can also be calculated by using a set of self-consistent linear equations.[22,23]

By changing the geometric parameters of the grooves, we can change the F fields inside the grooves and control the output field distribution furthermore. It is impossible to study all possible choices of the grooves. We focus on the periodic grooves in this paper. As Fig. 1 shows, all the grooves have the same shape with width $W_g=40$ nm and depth $h=100$ nm. The slit width is $W_s=40$ nm. All the grooves above the slit consist in the upper periodic grooves characterized by the initial location a_1 and the period b_1. The grooves below the slit are also periodic and the corresponding parameters are a_2 and b_2. When $a_1=a_2$ and $b_1=b_2$, the grooves are symmetric and we will use a and b to replace a_1, a_2 and b_1, b_2. The incident wavelength is $\lambda=560$ nm. In this paper, we try to find the best far-field oblique beaming at any given angle by modifying a_1, b_1, a_2, and b_2. Under the restriction of periodic grooves, we find an efficient algorithm to decide the parameters with an explicit physical explanation.

We begin our research by studying the F fields when the grooves are symmetric. Figures 2(a) and 2(b) show the amplitudes and phases of F_i when $a=b=500$ nm. All the F fields are normalized to the F field at the slit exit, so $F_0=1$. Figure 2(a) shows the field at the slit is much stronger than the fields at the grooves. The fields at the grooves decay

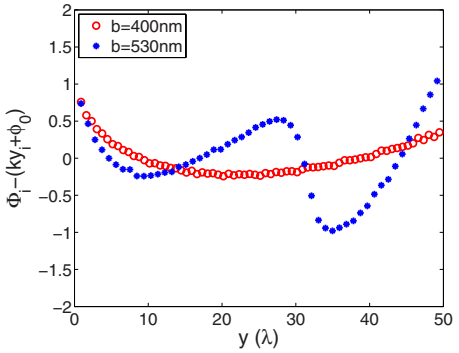

FIG. 3. (Color online) The fitting error of the phases of F_i when $a=500$ nm.

smoothly with the distance to the slit and become very weak in the end. There are 56 grooves in each side of the slit in this simulation. Further simulations show adding more grooves will not influence the far-field distribution much.

The most important property about the F fields is the perfect straight lines formed by the phases shown in Fig. 2(b). So we can use linear functions to fit them. For a positive integer i, the location of the ith groove is $y_i=a+(i-1)b$ and the phase is $\Phi_i=\mathrm{Arg}(F_i)$, then the linear function is

$$\Phi_i \approx ky_i + \phi_0. \tag{3}$$

This linear relation can be explained by the "single scattering approximation." The surface plasmons are excited at the exit of the slit and propagate along the output surface. Then they will interact with the grooves they meet. The weak F fields at the grooves suggest the interaction is weak. Most of the surface plasmons transmits through the grooves, so the F fields at grooves decay smoothly. Some is scattered into the free space and the rest is reflected. The single scattering approximation neglects the reflected surface plasmons. The surface plasmons repeat their behavior when they meet the next groove, so the phase change between two neighboring grooves is constant.

The single scattering approximation requires that the fitting parameters in Eq. (3) will not change with a. Our simulations confirm it. The fitting results are shown in Fig. 2(c) when $b=500$ nm and a changes from 200 to 1500 nm. We can see clearly that k is almost constant and ϕ_0 oscillates weakly.

Next we fix $a=500$ nm and change b from 100 nm to 1500 nm. The slope k in Eq. (3) is shown in Fig. 2(d). The wave vector of the surface plasmons is $k_{sp}=1.07k_0$. (The metal is gold and its permittivity is taken from Ref. 24.) We can find k is close to but not equals k_{sp}. It is because of the small phase change introduced by the grooves. When b increases, which means less grooves at the surface, k converges to k_{sp}.

The slope curve in Fig. 2(d) is bumpy when $kb \approx \pi n$ (n is an integer), which is because of "collective surface modes."[2] When $kb=\pi n$, the reflected surface plasmons from different grooves are in phase, so the single scattering approximation becomes weak. In Fig. 3, we plot the fitting error of the phases when $b=530$ nm and 400 nm. It is clear that the collective surface mode ($b=530$ nm) gives a bigger error.

Now we have understood the phase difference between two neighboring grooves is kb. If

$$kb - k_0 b \sin\theta = 2\pi n, \tag{4}$$

where n is an integer, all the grooves above the slit have constructive far-field interference at the angle θ. Figure 4(b) shows the constructive interference angles of the upper periodic grooves at different periods calculated from Eq. (4) based on the k in Fig. 2(d).

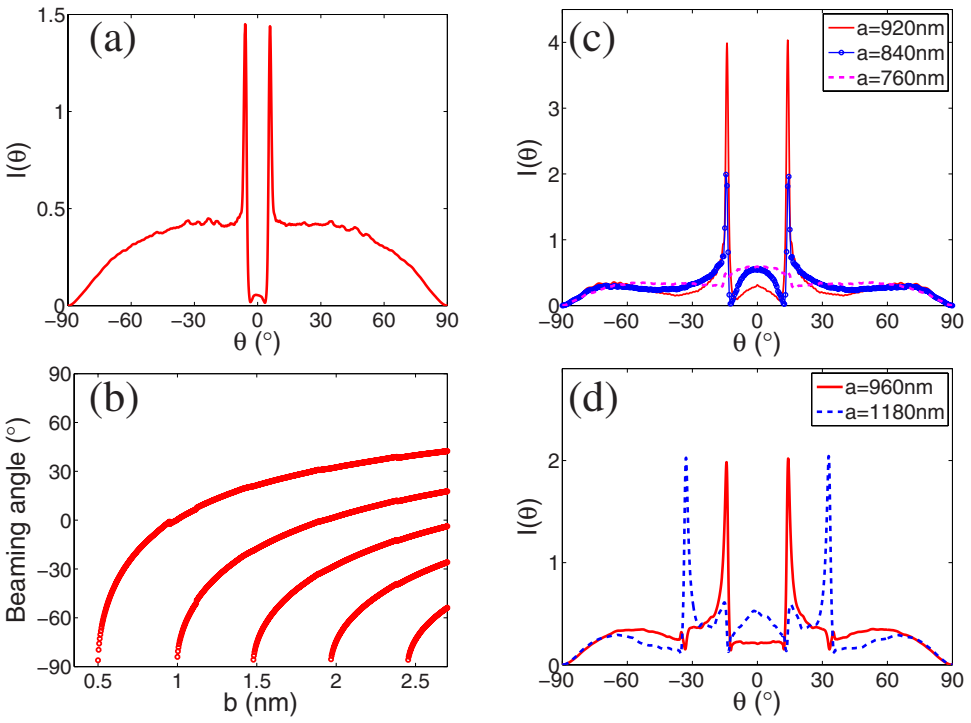

FIG. 4. (Color online) (a) Normalized far-field angular transmission when $a=b=500$ nm; (b) Constructive interference angles of the upper periodic grooves at different groove periods calculated from Eq. (4) when $n=1,2,\cdots,5$; (c) and (d) Normalized far-field angular transmission when $b=446$ nm and $b=710$ nm.

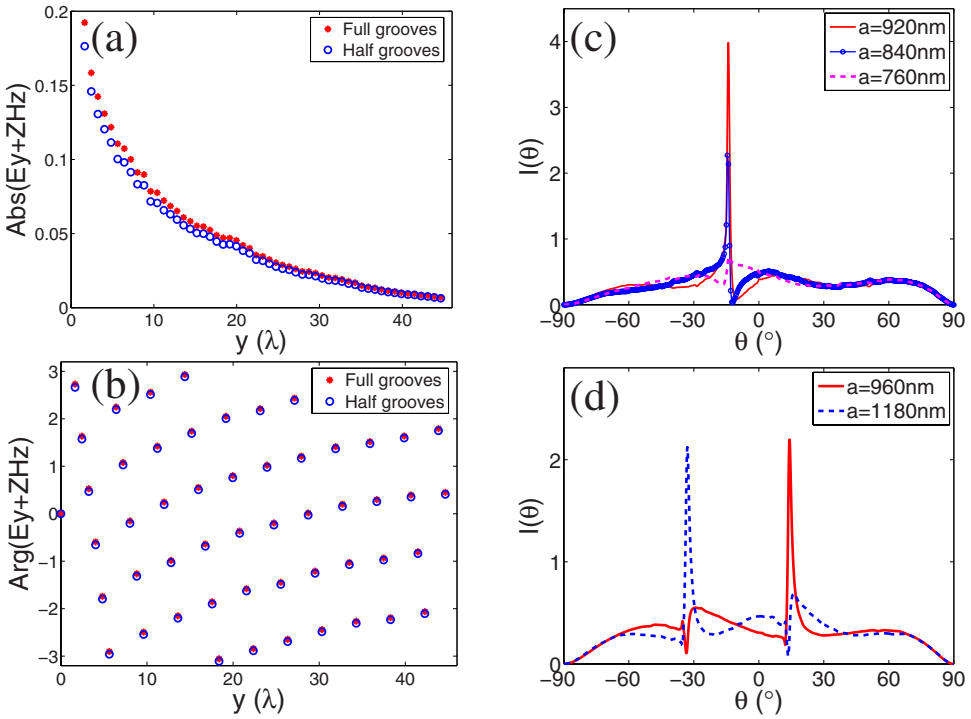

FIG. 5. (Color online) (a) and (b) Amplitudes and phases of fields at grooves above the slit when the grooves are symmetric with $a_1=a_2=920$ nm, $b_1=b_2=446$ nm and when there are only upper periodic grooves with $a_1=920$ nm and $b_1=446$ nm; (c) and (d) Normalized far-field angular transmission generated by the slit with upper periodic grooves alone when $b_1=446$ nm and $b_1=710$ nm.

We also calculate $I(\theta)$ from Eq. (2) when $a=b=500$ nm and the results are shown in Fig. 4(a). The normalized far-field angular transmission distribution curve has two peaks at $\pm 6°$, which equal the constructive interference angles of the upper and lower periodic grooves. When $b=530$ nm, the fitting error is bigger (shown in Fig. 3). But Eq. (4) still gives the right beaming angle, which is around 0°.

Besides the two peaks, the curve in Fig. 4(a) also has a smooth base, which is the contribution of the slit. The existence of the base means the energy is diffracted to all angles. So the strong filed in the slit deteriorates the directional emission. However, it also bring us the opportunity to control the peak heights. Considering the far-field interference between the slit and the upper periodic grooves at angle θ, the phase difference is $\phi_0+ka-k_0a \sin\theta$. So the peak heights change with a, as shown in Figs. 4(c) and 4(d).

Figure 4(c) also demonstrates the beaming angles are independent from a. A beaming angle is always a constructive interference angle of the upper or lower periodic grooves, which is decided by the period only. In Fig. 4(d), $b=710$ nm and the upper or lower periodic grooves have two constructive interference angles and the value of a decides which one becomes the beaming angle.

Until now we always use symmetric grooves, so the far-field distributions are also symmetric with two peaks. The ideal oblique beaming has only one peak. A nature idea is to remove all the grooves on the one side of the slit.[12]

Figures 5(a) and 5(b) show the amplitudes and phases of the F fields at the grooves above the slit when the slit is accompanied by the upper grooves only or by symmetric upper and lower grooves. The F fields under the two groove settings are quite close to each other, specially the phases. The similarity shows the independence between the upper and lower periodic grooves. The independence is also a nature result of the single scattering approximation. Since we neglect the reflected surface plasmons, the upward plasmons have no chance to reach the grooves below the slit, and vice versa. Ref. 12 also verified the independence between the upper and lower grooves. Figures 5(c) and 5(d) show $I(\theta)$ of a slit with upper periodic grooves alone when $b_1=446$ nm and $b_2=710$ nm. Comparing with Figs. 4(c) and 4(d), we can find that the absence of the lower grooves will not influence the peaks generated by the upper periodic grooves.

As Fig. 4(b) shows, when b_1 changes form 0.5λ to λ, the constructive interference angle changes from $-90°$ to $0°$. So we can always design an oblique beaming structure with the beaming angle at any angle. The structure is a subwavelength metallic slit with only the upper or lower periodic grooves. First we check Fig. 4(b) to get the period of grooves b_1 smaller than 540 nm. Then we fix the period and scan the initial location of the grooves a_1 to maximize the transmission peak height.

Figure 4(b) also shows when $b_1>540$ nm, the upper periodic grooves have several constructive interference angles and some of them are positive. Then the lower periodic grooves with period $b_2>540$ nm can have negative constructive interference angles. So it is possible that the upper and lower periodic grooves have the same beaming angles. Then we can design an oblique beaming structure using both upper and lower periodic grooves. Given an angle θ, we check Fig. 4(b) to find b_1 with the constructive interference angle θ and b_2 with the constructive interference angle $-\theta$. Then we study the angular transmission curves of a slit with upper periodic grooves alone. Fix the period as b_1 and scan a_1 to maximize the peak at θ. Repeat the process for b_2 to find the optimal a_2. Then all the four parameters a_1, a_2, b_1, and b_2 are obtained.

Figure 6 is an example of the algorithm. The beaming angle is $-14°$. From Fig. 4(b), we find the upper periodic

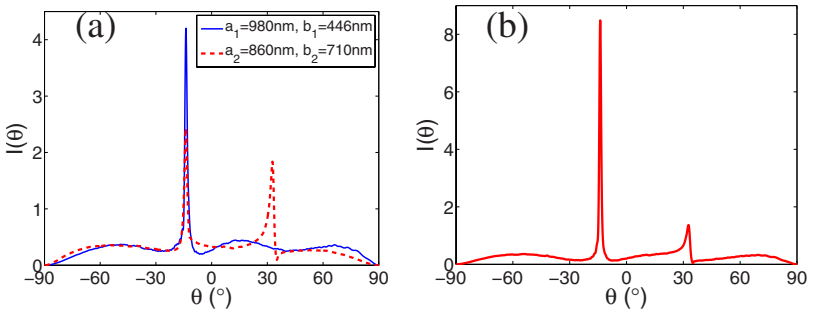

FIG. 6. (Color online) (a) Normalized far-field angular transmission of a slit with upper periodic grooves alone when $a_1=980$ nm, $b_1=446$ nm and a slit with lower periodic grooves alone with $a_2=860$ nm, $b_2=710$ nm; (b) Normalized far-field angular transmission of a slit with asymmetric upper and lower periodic grooves when $a_1=980$ nm, $b_1=446$ nm, $a_2=860$ nm, and $b_2=710$ nm.

grooves with $b_1=446$ nm and the lower periodic grooves with $b_2=710$ nm both have the constructive interference angle at $-14°$. Then we fix $b_1=446$ nm and calculate the normalized far-field angular transmission for different a_1. The highest peak is achieved when $a_1=980$ nm and the peak is shown Fig. 6(a). Repeat the process, when $a_2=860$ nm, the lower grooves with $b_2=710$ nm generate the highest peak at $-14°$. Then we put the upper and lower periodic grooves together. The far-field distribution of the slit surrounded by the asymmetric upper and lower grooves is shown in Fig. 6(b). Now all the three components, the upper periodic grooves, the lower periodic grooves and the slit, interfere constructively. So we get a higher far-field transmission peak at $\theta=-14°$ than the peaks in Fig. 6(a).

Figure 7 shows the properties of the highest transmission peaks we can achieve at different beaming angles using upper periodic grooves only or using asymmetric upper and lower periodic grooves based on the methods mentioned above. Adding grooves below the slit improves the transmission peaks. The highest peaks are achieved round 20°. When the beaming angle is big, cos θ in the numerator of Eq. (2) suppresses the peaks. When the beaming angle is small, the system is close to the collective surface modes. The fields in the grooves decay quickly[2] and the grooves tend to cancel each other because of the phases deviation from the linear relation. So the peaks of the normalized far-field angular transmission are low.

The shape of the grooves will also influence the quality of the beaming.[2] The fields at the grooves can be very weak given some special groove shapes. So the output field is decided by F_0 mainly and the beaming is suppressed. But the single scattering approximation tell us the shape effect is independent from a and b. So we choose h and W_g which give fairly strong fields at the grooves when $a=b=500$ nm. This groove shape also gives us good beaming for other a and b values as predicted.

We can also design a frequency splitter using asymmetric grooves: two close wavelengths enter the slit and leave at very different angles. We have understood the upper periodic groove has only one possible beaming angle when its period is smaller than the wavelength and the angle satisfies

$$kb - k_0 b \sin\theta = 2\pi. \tag{5}$$

The phase difference between the upper periodic grooves and the slit at the beaming angle is

$$ka + \phi_0 - k_0 a \sin\theta = 2\pi a/b + \phi_0. \tag{6}$$

We can find two wavelengths λ_1 and λ_2 satisfying $\phi_0(\lambda_1)-\phi_0(\lambda_2)=\pi$. When the upper grooves and slit interferes constructively at one wavelength, they have destructive interference at the other wavelength.

In Fig. 8(a), the two wavelengths are 650 and 695 nm. When the depth of grooves is $h=100$ nm, the difference between ϕ_0 at the two wavelengths is 1.7. To get bigger difference, we have to increase h to 500 nm. The period of the upper periodic grooves is $b_1=500$ nm. The constructive interference angles of the upper grooves are around $-17°$ for both wavelengths. But because of the interference between the upper grooves and slit, only the field with $\lambda=650$ nm has a transmission peak at its constructive interference angle. For the lower periodic grooves, we choose $b_2=b_1$ and a different a_2 to enhance the peak $\lambda=695$ nm. Though the two incident wavelengths are quite close to each other, the angular transmission peaks are 34° away from each other.

Based on Eqs. (5) and (6), if we change b but keep a/b unchanged, the location of the peak changes but the phase

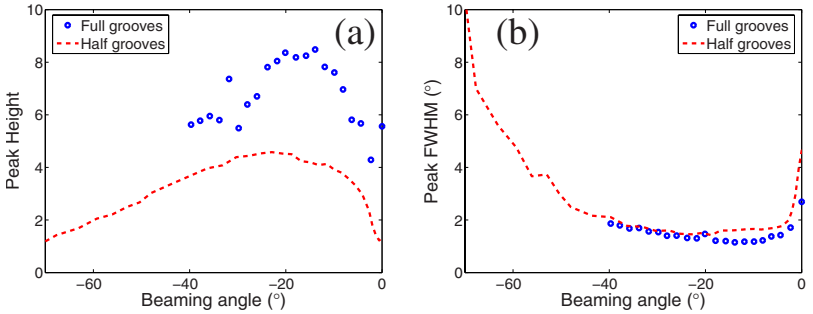

FIG. 7. (Color online) (a) Heights and (b) full widths at half maximum of the highest far-field transmission peak at different angles generated by upper periodic grooves only and asymmetric upper and lower periodic grooves. The working wavelength is $\lambda=560$ nm. The grooves have the width $W_g=40$ nm and depth $h=100$ nm. The width of the slit is $W_s=40$ nm. a_1, a_2, b_1, and b_2 are optimized for each beaming angle using the algorithms presented in this paper.

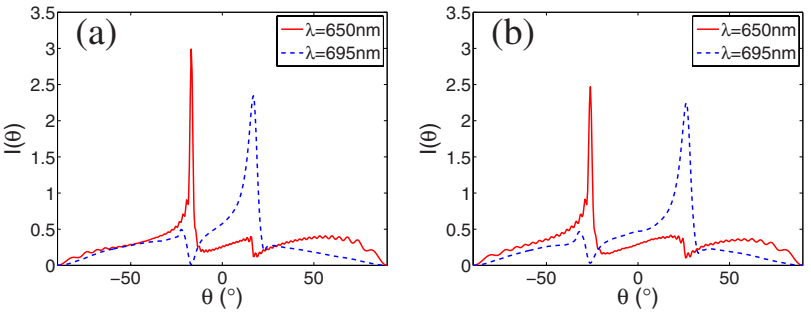

FIG. 8. (Color online) Normalized far-field angular transmission at two frequencies when (a) a_1=600 nm, b_1=500 nm, a_2=400 nm, and b_2=500 nm, and (b) a_1=540 nm, b_1=450 nm, a_2=360 nm, and b_2=450 nm. The groove depth is h=500 nm.

difference between the grooves and the slit at the peak angle don't. In Fig. 8(b), a_1, a_2, b_1, and b_2 are 10% smaller then the corresponding values in Fig. 8(a). The structure still works as a frequency splitter and the output peaks are 52° away.

In this paper, we implement good oblique beaming at any angle in the range of ±70° using a metallic subwavelength slit with one-side periodic grooves and better oblique beaming at an angle between ±40° using a slit surrounded by upper and lower periodic grooves. We also design a frequency splitter using this kind of structures.

Work at Ames Laboratory was supported by the Department of Energy (Basic Energy Sciences) under Contract No. DE-AC02–07CH11358. This work was partially supported by the AFOSR under MURI grant (Grant No. FA9550–06–1-0337).

*soukoulis@ameslab.gov

[1] H. J. Lezec, A. Degiron, E. Devaux, R. A. Linke, L. Martín-Moreno, F. J. García-Vidal, and T. W. Ebbesen, Science **297**, 820 (2002).
[2] L. Martín-Moreno, F. J. García-Vidal, H. J. Lezec, A. Degiron, and T. W. Ebbesen, Phys. Rev. Lett. **90**, 167401 (2003).
[3] F. J. García-Vidal, L. Martín-Moreno, H. J. Lezec, and T. W. Ebbesen, Appl. Phys. Lett. **83**, 4500 (2003).
[4] D. Z. Lin, C. K. Chang, Y. C. Chen, D. L. Yang, M. W. Lin, J. T. Yeh, J. M. Liu, C. H. Kuan, C. S. Yeh, and C. K. Lee, Opt. Express **14**, 3503 (2006).
[5] B. Wang and G. Wang, Appl. Phys. Lett. **88**, 013114 (2006).
[6] P. Wróbel, J. Pniewski, T. J. Antosiewicz, and T. Szoplik, Phys. Rev. Lett. **102**, 183902 (2009).
[7] E. Moreno, F. J. García-Vidal, and L. Martín-Moreno, Phys. Rev. B **69**, 121402(R) (2004).
[8] P. Kramper, M. Agio, C. M. Soukoulis, A. Birner, F. Müller, R. B. Wehrspohn, U. Gösele, and V. Sandoghdar, Phys. Rev. Lett. **92**, 113903 (2004).
[9] S. K. Morrison and Y. S. Kivshar, Appl. Phys. B: Lasers Opt. **81**, 343 (2005).
[10] R. Moussa, B. Wang, G. Tuttle, T. Koschny, and C. M. Soukoulis, Phys. Rev. B **76**, 235417 (2007).
[11] W. Dai and C. M. Soukoulis, Appl. Phys. Lett. **93**, 201101 (2008).
[12] J. Bravo-Abad, F. J. García-Vidal, and L. Martín-Moreno, Photonics Nanostruct. Fundam. Appl. **1**, 55 (2003).
[13] S. Kim, H. Kim, Y. Lim, and B. Lee, Appl. Phys. Lett. **90**, 051113 (2007).
[14] H. Caglayan, I. Bulu, and E. Ozbay, J. Appl. Phys. **104**, 073108 (2008).
[15] H. Caglayan, I. Bulu, and E. Ozbay, Appl. Phys. Lett. **92**, 092114 (2008).
[16] E. Ozbay, Science **311**, 189 (2006).
[17] F. J. García-Vidal, H. J. Lezec, T. W. Ebbesen, and L. Martín-Moreno, Phys. Rev. Lett. **90**, 213901 (2003).
[18] O. T. A. Janssen, H. P. Urbach, and G. W. 't Hooft, Phys. Rev. Lett. **99**, 043902 (2007).
[19] N. Yu, J. Fan, Q. Wang, C. Pflüg, L. Diehl, T. Edamura, M. Yamanishi, H. Kan, and F. Capasso, Nat. Photonics **2**, 564 (2008).
[20] S. Kim, Y. Lim, H. Kim, J. Park, and B. Lee, Appl. Phys. Lett. **92**, 013103 (2008).
[21] J. Jackson, *Classic Electrodynamics*, 3rd ed. (Wiley, New York, 1998).
[22] F. López-Tejeira, F. J. García-Vidal, and L. Martín-Moreno, Phys. Rev. B **72**, 161405 (2005).
[23] W. Dai and C. M. Soukoulis, Phys. Rev. B **80**, 155407 (2009).
[24] E. D. Palik, *Handbook of Optical Constants of Solids* (Academic, New York, 1985).